Proceedings of the
Annual Stability Conference
Structural Stability Research Council
Baltimore, Maryland, April 10-13, 2018

Modal interaction in design of improved stiffened trapezoidal profiled sheeting: shape grammar, elastic stability and strength analysis

Juarez M.S. Franco[1], João P.M. Garcia[2], Eduardo M. Batista[3]

Abstract
The main goal of the present research is to investigate a procedure to design of improved stiffened trapezoidal profiled sheeting. In recent work, the authors have combined shape grammar and linear elastic analysis in a semi-automatic procedure to achieve improved solutions with a fitness function based on flexural bending moment critical values (top compression and bottom compression). The profile's signature curves presented the interesting characteristic of three minimum with equivalent critical values, which suggests the possibility of strength erosion by modal interaction. Two questions have been proposed: (i) what the amount of strength erosion is induced by modal interaction in "best shapes" from elastic stability criteria, (ii) how to find solutions where this interaction has less pronounced effects in the neighborhood of the best shapes. Two procedures were performed to answer these questions: (a) the semi-automatic shape grammar procedure keeps the records from the start point to best solution, which leads to identify how geometric parameters induces buckling modes with a certain difference of critical values. Many solutions were tested and compared with results from closed formulae of Direct Strength Method to measure strength erosion and (b) Direct Strength Method has been implemented in the semi-automatic procedure Shape Grammar / Linear Elastic Stability Analysis where Local and Distortional buckling modes are identified by half-wave length criteria, according to experience in similar problems; after this, best solutions were investigated in detail by non-linear elasto-plastic analysis in Finite Element Method. There are some possible conclusions from comparisons: if procedures (a) and (b) achieves the same result ("best" shape), so Direct Strength Method is properly calibrated for these cold-formed sections and the procedure (b) is most appropriate because requires less computational effort; else, it may be necessary to choose between computational or manufacturing costs. Finally, if results from Finite Element Analysis and Direct Strength Method diverge, more research will be necessary.

1. Introduction
Thin-walled steel trapezoidal profiled sheeting (TPS) is a traditional solution to large span roofing systems. The present work is addressed to improve the strength of TPS cold-formed steel section (simply supported beam subject to uniform bending and free warping end conditions).

[1] Adjunt Professor, Federal Rural University of Rio de Janeiro, <juarezfranco@ufrrj.br>
[2] Master Graduate Student, Federal University of Rio de Janeiro, <joaopedro@coc.ufrj.br>
[3] Associate Professor, Federal University of Rio de Janeiro, <batista@coc.ufrj.br>

This typology, as many others cold-formed steel members, presents slender open cross-sections and has a complex behavior involving Local (L) and Distortional (D) buckling modes. At this work, critical buckling moments are called M_{crL} (local instability from shorter lengths) and M_{crD} (distortional instability from intermediate lengths). Global instability from larger lengths, $M_{crG,}$ has not been relevant in this paper, because M_{crG} / $M_{cr.max}$ >> 1 on the investigated span range (where $M_{cr.max} =$ max {$M_{crL,}$ M_{crD}}). When M_{crL} and M_{crD} are close enough, there is the possibility of L-D interaction. Recent works (Martins et al. 2017) have done an L-D interaction study on beams for lipped channels, zed-sections and hat sections, but we didn't locate in-deep numerical and experimental investigations of the same phenomena for TPS. This way, our work presents a very preliminary study of significant M_{crL}/M_{crD} ratios ($R_{DL)}$ in design of thin-walled steel trapezoidal profiled sheeting beams. A numerical study over many geometrical parameters has been carried out, in order to (i) estimate significative evaluate strength erosion from modal interaction effect and (ii) identify a simplified process to define the more efficient shapes from a manufacturer point of view and small computational costs. This task was achieved with the help of rational combination of shape grammar procedure, elastic buckling analysis and structural strength identification.

The research on trapezoidal profiled sheeting beams (TPS) has some particularities: (i) the number of geometric variables required to the specification of TPS is greater than other conventional shapes. For instance, lipped channels, zed-sections and hat sections have proportions between the walls that ensure the predominance of Local (L), Distortional (D) or Global (G) buckling mode over the others. TPS are specified by a relatively high number of geometric parameters and admits a huge variety of subtypes, making the identification of proportions and angles between walls excessively cumbersome and potentially imprecise; (ii) the lack of publications on experimental campaigns in TPS makes it practically impossible to validate the numerical results obtained in this research.

The Fig. 1 shows an example of thin-walled steel trapezoidal profiled sheeting (TPS) structural member. The usual way to improve its structural performance is to adopt stiffened section obtained by continuous cold rolling manufacturing. In this case, there are many types of stiffeners, offering distinct structural performance regarding local buckling effects. Previous work (Franco and Batista 2017) showed the effect of the variation of the geometry, dimensions and distribution of intermediate stiffeners, as well as dimension proportion between plate elements and the web angles regarding the buckling performance. These initial results highlighted the main aspects for the M_{crL} and M_{crD} improvement of the stiffened trapezoidal sections.

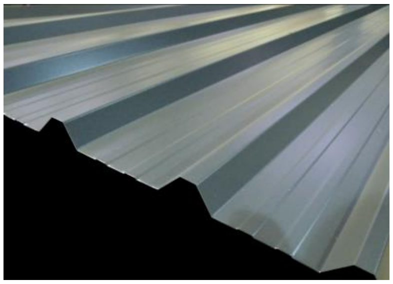

Figure 1: Steel trapezoidal profiled sheeting beams conforming orthotropic roofing system (https://www.cladco.co.uk/products/box-profile-321000-sheets-roofing-and-cladding)

TPS design procedures may be organized by adopting FEM for both elastic buckling analysis and geometrically imperfect nonlinear material structural analysis for bending strength. Although available in usual FEM packages, this type of numerical analysis results too much time consuming and, in addition, is not acceptable for regular structural design (although very much useful for investigation purposes). Direct Strength Method (AISI 2006) is a possible alternative by the following steps: (i) identification of the elastic critical buckling bending moments and modes classification (local or distortional, respectively *L* or *D*, since global mode *G* is not expected in the present case), (ii) applying direct strength equations previously calibrated to obtain the bending moment resistance. In this case, FEM may be avoided and finite strip method (FSM) or GBT-based computational programs are available for the buckling analysis, converging for a much more attractive (accurate and much less time consuming) solution of the problem. However, a major point must be considered in the present case: known Direct Strength Method (DSM) equations are calibrated for specific geometrical limitations for the case of trapezoidal profiled sheeting pre-qualified beams (AISI 2006), which are not respected in many cases of the developed stiffened CFS.

A partial response addressed to the improvement of stiffened trapezoidal members of orthotropic roofing system is a combination of the FSM and shape grammar (Franco and Batista 2017). The authors defined a rational sequence of procedures aiming at improvement the critical buckling bending moments for both cases of uplift and down lift loading (bottom and top flanges compression, respectively), avoiding optimization techniques. Although the obtained results identified trapezoidal sections with the better results concerning elastic buckling moments, two additional questions remain opened: (i) bending strength was not computed due to lack of confirmation if the DSM equations are consistent for the conceived geometries (many of them does not respect pre-qualified beams geometry), (ii) local or distortional (*L* or *D*) buckling modes conduct to different strength results and this is especially true for the case of distortional buckling including out of plane displacements of the intermediate stiffeners, for which we find scarce experimental results in the literature.

The structural strength of compressed cold-formed plate elements with intermediate stiffeners may be accessed with the help of the effective width procedure described in international standards (AISI 2006, Eurocode 2004), but these are not attractive solutions to be considered. DSM-based solution would serve much better in this case. In addition, the effect of the buckling modes interaction must be carefully observed, considering the improved stiffened trapezoidal cross-section previously developed (Franco and Batista 2017) displays clear coincidence of the critical bending moment for distinct buckling modes displaying short and much longer semi-waves lengths. This aspect of the problem is not available in the literature and merits deeper investigation.

2. Beam geometry parameters, fitness functions and procedures

A basic unstiffened trapezoidal CFS shape is illustrated in Fig. 2 including details of a (hypothetical) self-tapping screw connection with the adjacent members, as well as a protection cap. The usual solution is the adoption of internal stiffeners as presented in Fig. 3, with possible variation of the stiffeners geometry itself as well as its distribution along the plate elements of the CFS.

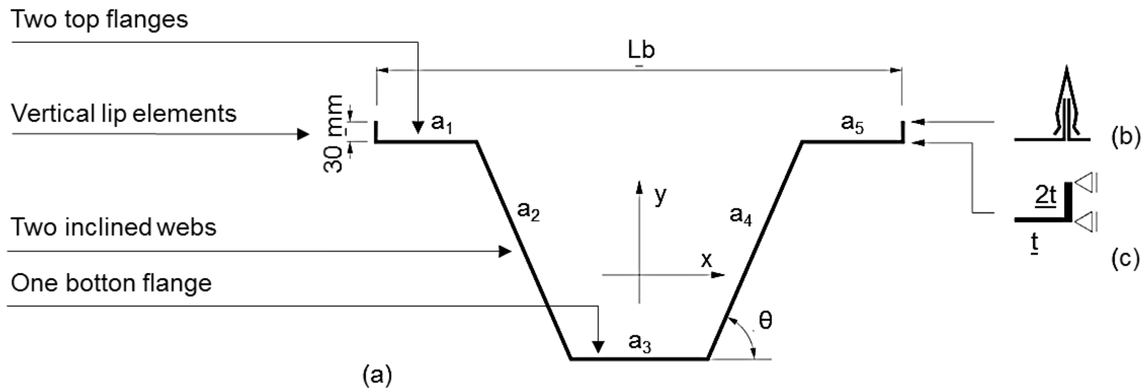

Figure 2: (a) Unstiffened trapezoidal CFS, (b) hypothetical screw connection between trapezoidal members, (c) admitted support conditions for the buckling analysis

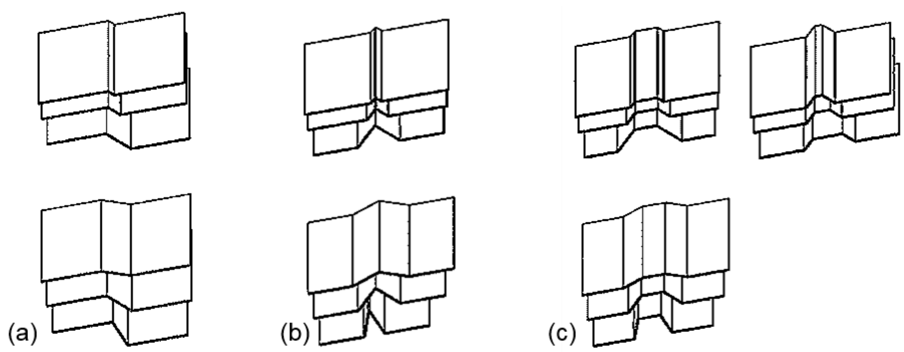

Figure 3: Geometry variation of intermediate stiffeners w_i and ang_i, measured by the cross-section mid line: (a) two, (b) three and (c) four folded corners stiffeners

Fixed geometrical properties of the trapezoidal CFS, hereafter named as essential properties, are: (i) mono-symmetrical cross-section, (ii) two top flanges, (iii) one bottom flange, (iv) two inclined webs, (v) two 30mm width vertical lip elements on the free edges of the top flanges (screw connection positions). The variable geometrical properties of the trapezoidal CFS, hereafter named as accidental geometrical characteristics, are: (i) web angle Θ; (ii) flanges and webs widths and (iii) the presence of the intermediate stiffeners illustrated in Fig. 3. The development of stiffened trapezoidal CFS was considered with the following conditions: (i) original steel sheet coil width is L_s=1200mm based on actual manufacturing condition, (ii) steel sheet thickness is 0,8, 1,0, 1,5 and 1,55mm, (iii) intermediate stiffeners. The main accidental geometric parameters of the stiffeners are the element width w_i and angle ang_i (see Fig. 3). The effectiveness of the stiffeners is associated with its capacity to improve the CFS buckling behavior, which depends on (i) the geometry of each single folded stiffener, (ii) the combination of different stiffeners in a single CFS and (iii) the number and distribution of the internal stiffeners along the cross-section.

Buckling analysis covers two directions of the bending moment (both around the centroid horizontal axis X): (i) gravity direction transversal loading, typical of the structure self-weight combined or not with water blade and (ii) lifting effect due to wind forces. Considering simply supported spans with no cantilevers, the former leads to compression in the top flange (TC: top flange compression) and tensile stresses in the bottom flange, the latter promotes contrary effects with compression in the bottom flange (BC: bottom flange compression). In this condition, an uplift wind effect is the major live loading to be considered for the design of the roofing system (when no snow loading is considered). The identification of the best CFS shapes based on buckling analysis can be considered as a valuable point of departure to rank the cross-section structural performance. The analysis for both elastic buckling and strength must take into consideration the flexural behavior of the stiffened trapezoidal CFS in both upward and downward directions, which will be identified hereafter as “bottom" or “top" compression flange bending moment, M^{BC} and M^{TC} respectively. Consequently, the fitness function to be evaluated are (i) the elastic critical buckling for top and bottom compression, respectively M_{cr}^{TC} and M_{cr}^{BC}, and (ii) the covering width L_b (see Fig. 2). Improved trapezoidal corrugated CFS for roofing purposes must attend balanced results that include both the cross-section strength and its roof covering capacity. A covering rate $C_{ov}= L_b/L_s$ was adopted as the ratio between the roof covering width of a single trapezoidal CFS L_b and the original coil width L_s=1200mm.

3. Elastic Buckling Analysis and Parametric Shape Grammar

Based on Generative Grammar (Chomsky 1972) and Shape Grammar (Stiny and Gips 1972), Franco et al. (2014) developed an original cold-formed section grammar system, CFS Grammar, dedicated to generating all manufacturable steel CFS. As mentioned before, constant geometrical characteristics of the CFS are named essential properties and those to be submitted to variation are named accidental properties. CFS Grammar has been designed as a “generative system of all feasible shapes from manufacturing point of view and none infeasible". This subset of shapes is identified by B in Fig. 4(a*).* The set of all shapes includes infeasible solutions, represented by A in the same diagram. Subset C represents only standard shapes provided by producer's records. The specialized generative system of the present investigation is derived from the general CFS Grammar, as illustrated in Fig. 4(b). This tool is useful to investigate typologies with high numbers of geometric parameters.

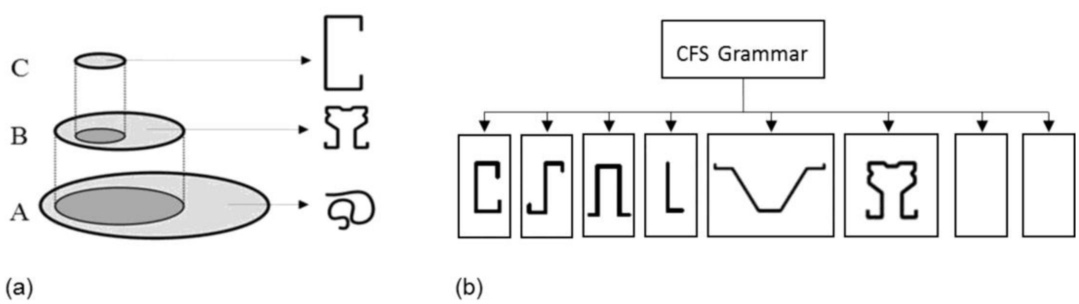

Figure 4: (a) CFS Language as a subset of all feasible CFS shapes, (b) definition of the CFS Grammar to create any typology of CFS

The starting point of the series of trapezoidal CFS computational generation and buckling analysis is the unstiffened section with geometrical parameters defined in an arbitrary way. The obtained results are transferred to the next step of the “computational geometric generation and buckling analysis" procedure. The automated calculation sequence is intended to generate (i) controlled trapezoidal CFS, (ii) automatically produce data to CUFSM computational program, (iii) run finite strip method buckling analysis and (iv) collect the buckling analysis results. The developed procedure permits to obtain large and organized computational results with high efficacy. The description and results obtained by means of this procedure are presented in previous work (Franco and Batista 2017).

The buckling modes of the stiffened trapezoidal CFS are identified with the help of the finite strip method computational program CUFSM (Li and Schafer 2010). Initially, up to three TPS beams were considered connected side by side for the analysis and it was found that a single trapezoidal CFS can be admitted, with nearly the same results as those found with two and three members. Consequently, single CFS's were taken for the buckling analysis with the following conditions included in the model: (i) simply supported and free warping at the end sections of the trapezoidal members, the usual condition for deep trapezoidal roofing members, (ii) fixed horizontal displacements condition and double thickness in the 30mm width top vertical lips with screw connection (see Fig. 2(c)), (iii) folded corners are admitted with no internal radius for the numerical analysis, (iv) all dimensions are related to the mid line of the CFS plate elements, (v) steel elastic properties are the modulus of elasticity E=205GPa and the Poisson ratio v=0,3. These are idealized conditions to achieve buckling analysis equivalent to the orthotropic roofing system.

The classification of the buckling modes as local or distortional was decided by inspecting the modes shape and wave lengths instead of by automatic identification displayed by the computational program CUFSM because a kind of "uncertainty in the definition of buckling modes of thin-walled members" has been pointed in literature (Adany 2004), especially in case of intermediate stiffeners, where walls are close to collinear or too small. This study has avoided in-deep discussion about this kind of uncertainty and assumes local instability from shorter lengths and distortional instability from intermediate lengths. Besides that, there is no "pure modes" (Fig. 05 and 06) computation in this approach. From a large collection of results, one may find single local and three distinct distortional buckling modes in the case of top flange compression produced by M^{TC} bending moment. Fig. 5 displays these buckling modes: (a) short semi-wave local plate TL, (b) distortional buckling promoted in the web (plate element with multiple stiffeners) TDW, (c) longer semi-wave distortional buckling promoted in the compressed flange TDF, (d) much longer semi-wave for the case of cross-section distortional buckling TD (in this case results are only obtained with twin trapezoidal CFS).

The Fig. 6 displays the results of the buckling analysis for the case of bending moment producing bottom flange compression, M^{BC}: (a) BL is a short semi-wave length local buckling, (b) BDF is the distortional buckling promoted in bottom compressed flange, (c) BDW is the distortional buckling started in the stiffened webs. Differently from the case of top flange compression distortional buckling TD, the distortional buckling mode BD presented in Fig. 6(d) was identified as dominant (critical) in many cases of the stiffened trapezoidal members.

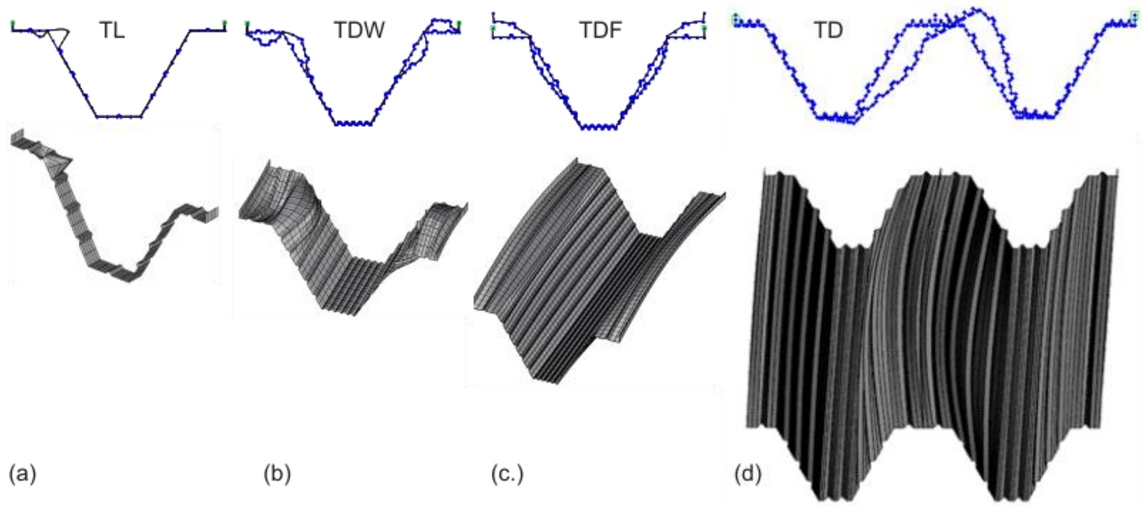

Figure 5: Local and distortional buckling modes of trapezoidal profiled sheeting for top flange compression: (a) local mode TL, (b) distortional web mode TDW, (c) distortional flange mode TDF, (d) distortional mode TD

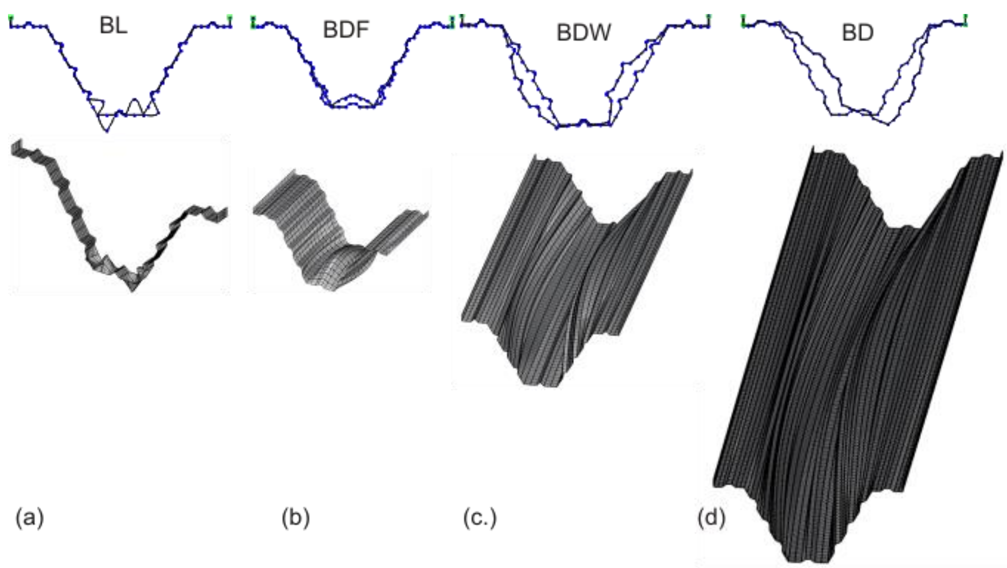

Figure 6: Local and distortional buckling modes of trapezoidal profiled sheeting for bottom flange compression: (a) local mode BL, (b) distortional flange mode BDF, (c) distortional web mode BDW and (d) distortional mode BD

As previously reported by the authors (Franco and Batista 2017), shape grammar (Franco et al. 2014) and constrained finite strip method (Li and Schafer 2010) were combined in the computational search procedure in order to find improved stiffened trapezoidal cross-sections, which means as higher as possible critical bending moments including both up and down wind effect – bottom and top cross-section compression, respectively. In addition, the roofing coverture L_b (see Fig. 2) must be considered, represented by the coverture ratio $Cov=L_b/L_s$.

The obtained results (Franco and Batista 2017) indicated the trapezoidal section shown in Fig. 7(a, b, c) as the best choices taking into consideration the following conditions and results: (i) original steel coil width $L_s=1200mm$ and thickness $t=1{,}0mm$, (ii) steel properties are $E=200GPa$, $\nu = 0{,}3$, (iii) web angle $\theta=60^o$ or 72^o, (iv) four folded corners stiffeners with wall widths $w_i=19mm$ and angle $ang_i=40^o$, (v) stiffeners distribution is one in top and one in bottom flanges, and three uniformly distributed stiffeners in each web.

The results included in Fig. 7(d) shows the variation of the critical buckling moments for top and bottom compression condition, M_{cr}^{TC} and M_{cr}^{BC} respectively, according with the web angle θ (from 30^o to 90^o). One may observe the best results in terms of the critical buckling bending moments is $\theta=72^o$, in this case associated with poor coverture result, with $Cov=0{,}5$ as confirmed in Fig. 7(e). In order to accomplish $Cov \geq 0{,}6$ as a minimum acceptable result (a target condition), web angle $\theta=60^o$ was elected the best choice in the present case, as presented in Fig. 7(d, e).

The structural performance of the trapezoidal member presented in Fig. 7(a), with web angle $\theta=60^o$, is illustrated in Fig. 8 by its signature curve obtained with the help of CUFSM computational program, concerning bending moments with bottom flange compression (this was the main loading condition in the present case). These results indicate the elastic buckling behaviour with three critical buckling modes: $M_{cr}^{BC}=34{,}78kNm$ for $L_{cr}=41mm$; $M_{cr}^{BC}=36{,}46kNm$ for $L_{cr}=1048mm$; $M_{cr}^{BC}=34{,}69kNm$ for $L_{cr}=4292mm$. These buckling modes were identified respectively as local plate *BL*, web distortional buckling *BDW* and distortional *BD*. The signature curve also allows us to identify *BL* as a very short semi-wave local buckling mode, *BDW* with longer semi-wave local buckling mode (L_{cr} is *25* times *BL* semi-wave length) for which the stiffeners move out of the plate and *BD* is typically a distortional buckling mode with much longer semi-wave (L_{cr} is *105* times *BL* semi-wave length).

The presented results indicate nearly the same value for the three critical bending moments and, in addition, associated to very short, longer and much longer semi wave modes, a probable deleterious effect for the cross-section bending strength due to buckling modes interaction.

4. "Best geometry" from buckling-based procedure

FEM model was applied to investigate the cross-section bending moment strength of the stiffened trapezoidal profiled sheeting originally developed and reported in the previous sessions. For this, the following computational resources were considered: (i) FEM computation with the help of Ansys program (SAS 2015), (ii) Shell 181 finite element, considered adequate for linear and nonlinear analysis of thin-walled members with reduced integration technique. Elastic analyses were implemented with Poisson ratio ν=0,3 and modulus of elasticity E=205GPa, following previous conditions adopted by the authors. Ductile material was modeled based on bi-linear stress-strain law, taking two different values of the yield stress, depending of the type of analysis, as will be explained later: fy=350 MPa or 600MPa.

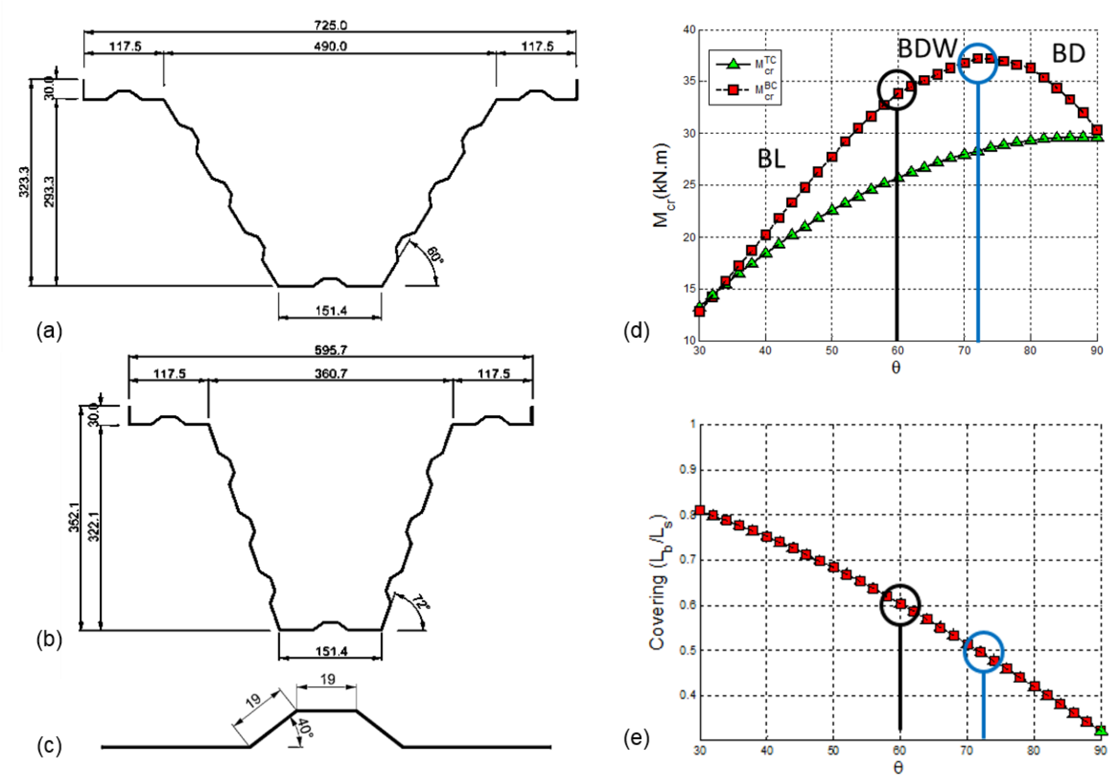

Figure 7: Stiffened trapezoidal sections with best structural performance (Franco and Batista 2017): (a) web angle θ=60°, (b) web angle θ=72°, (c) geometry of the best choice of intermediate stiffener, (d) results of the critical buckling bending moments for top and bottom compression, M_{cr}^{TC} and M_{cr}^{BC}, according with web angle variation, (e) covering ratio according with web angle variation

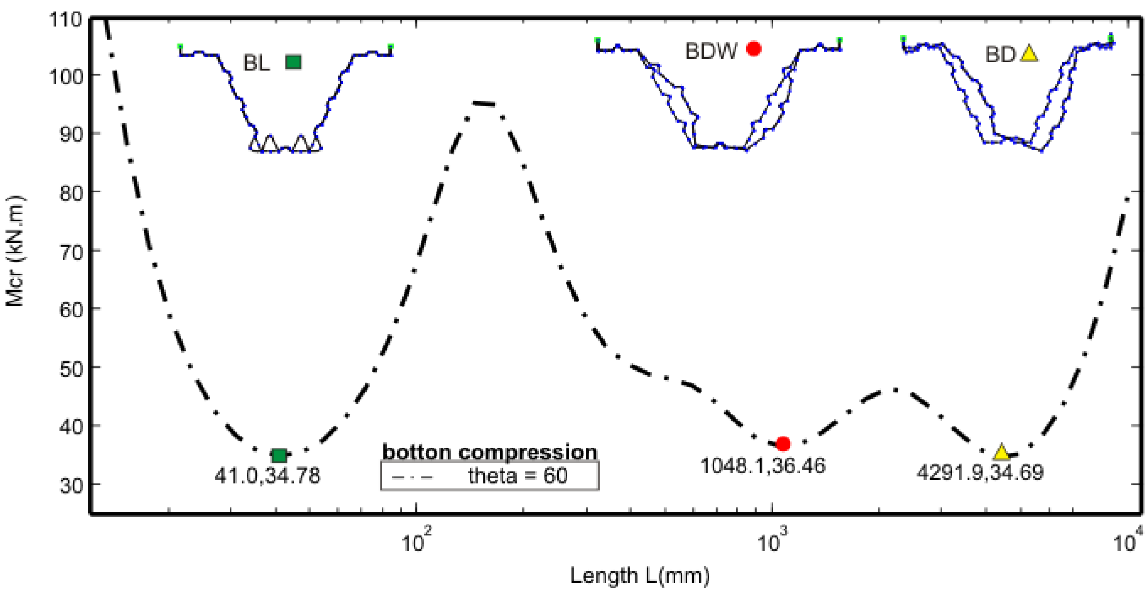

Figure 8: Improved stiffened trapezoidal profiled sheeting with the cross-section shown in Fig. 7(a) and web angle ϴ=60°: buckling modes signature curve computed from CUFSM

Finite element mesh was developed with *10x10x1mm* 181 shell elements (this choice resulted in accurate enough results for both linear and nonlinear analyses). In addition, two distinct numerical solutions were implemented: (i) first order elastic buckling analysis and (ii) geometrically imperfect nonlinear material structural analysis for bending strength identification. FEM buckling analysis results were compared with those from the computational program CUFSM, in order to confirm the actual buckling modes to be considered. The nonlinear analysis was performed taking into consideration: (i) Newton-Raphson incremental method, combined with arc length strategy, allowing identification of the limit value - the bending moment strength of the cross-section, (ii) geometrical initial imperfections on the basis of the previously computed buckling modes, (iii) maximum amplitude initial imperfection is *0,1* times the plate thickness *t*. Higher yield stress, $f_y=600MPa$, was adopted to generate more slender sections, permitting following the buckling modes in large displacements, as well as observing the development of localized plate collapse mechanism. Regular yield stress, $f_y=350\ MPa$, was considered to obtain actual flexural strength for the case of standard structural steel applied in manufacturing stiffened profiled sheeting.

Finally, the displacement restrictions of the FEM model considered: (i) simply supported beam behavior, (ii) free warping at the end sections, (iii) vertical lips in the top flange (screw connection shown in Fig. 2(b)) continuously restrained against lateral displacements along the member length (the same restriction condition adopted in the FSM computation, as illustrated in Fig. 2(c)).

The results of the numerical analysis will be presented, addressed to the stiffened trapezoidal profiled sheeting described in Fig. 7(a), for $\theta=60^o$, that was designed as the best choice after combined FSM buckling analysis and shape grammar procedure.

The *Table 1* shows the results of the buckling analysis from both FSM and shell FEM computation, from which one may observe good agreement (maximum difference is *7%* for the case of *BDF*). For this, the finite element computation was implemented with member length *L* equal to three buckling semi-waves, derived from the previous FSM results. In addition, the obtained buckling modes will define the initial geometrical imperfections for nonlinear analysis, as described in the next session.

Table 1: Critical buckling bending moment (kNm) for bottom compression bending, M_{cr}^{BC}

Buckling modes (according with *Fig. 6*)	M_{cr}^{BC} (FSM)	M_{cr}^{BC} (FEM)	FEM/FSM
BL	34,78	33,94	0,98
BDW	36,47	34,39	0,94
BDF	50,51	47,06	0,93
BD	39,40	37,42	0,95

The ultimate bending moment - formally the flexural strength of the section - was obtained with the help of the finite element nonlinear analysis model described in session 4.1, taking into account high yielding strength, f_y=600 MPa, and regular steel properties, f_y=350MPa.
Table 2 shows the results for the four buckling modes, for bottom compression loading case: (i) the computed member length $L=3.L_{cr}$, (ii) the initial yielding bending moment $M_y^{BC}=S_x.f_y$ (for

fy=350 or 600MPa), (iii) the critical buckling moment, M_{cr}^{BC}, (iv) the section slenderness according with Eq. (1), for each buckling mode λ_{BL}, λ_{BDW}, λ_{BDF} and λ_{BD}, (v) the obtained ultimate bending moment (flexural strength) for bottom compression loading case, M_R^{BC}.

$$\lambda_{BL} = \sqrt{\frac{M_y}{M_{cr,BL}}} = \sqrt{\frac{f_y}{\sigma_{cr,BL}}} \tag{1}$$

Table 2: FEM nonlinear analysis results of the flexural strength M_R^{BC} (kNm)

Buckling modes (*Fig. 6*)	L=3.L_{cr} (mm)	M_y^{BC} f_y=350MPa	M_y^{BC} f_y=600MPa	M_{cr}^{BC} (FEM)	λ f_y=350MPa	λ f_y=600MPa	M_R^{BC} f_y=350MPa	M_R^{BC} f_y=600MPa
BL	123	31,34	53,72	33,94	0,96	1,26	29,44	38,96
BDW	3144	31,34	53,72	34,39	0,96	1,25	29,70	33,46
BDF	1347	31,34	53,72	47,06	0,82	1,07	30,16	35,68
BD	12873	31,34	53,72	37,42	0,92	1,20	NA	NA

The Fig. 9 shows the nonlinear analysis results: load vs. displacements curve and the collapse mechanism for buckling modes BL, BDW and BDF. Buckling mode BD needs quite long member (too much computational effort) and because of this, the numerical results were not yet available.

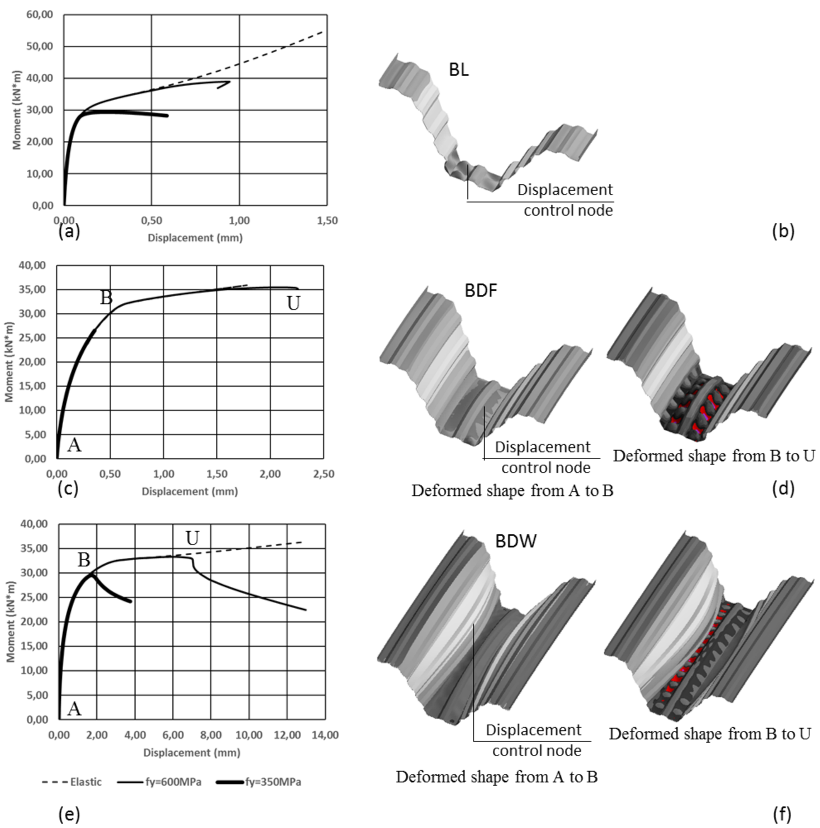

Figure 9: FEM nonlinear analysis results for the considered buckling modes: BL, BDF, BDW

Direct strength method equations found in the AISI standard (AISI 2006) were applied for each case of the flexural strength included in Tab. 2. The results are included in Tab. 3, as well comparison between DSM and FEM numerical results.

The present results and comparisons between DSM and FEM shows adequate accuracy (*0,93* to *1,06* ratio), exception for the case of BDW and slenderness factor $\lambda_{BDW}=0,96$, for which DSM result is *15%* below FEM one. These are promising results but it is clear that more results – both numerical and experimental - are needed to support conclusions about flexural strength of thin-walled stiffened profiled sections.

5. A first approach for modal interaction in improved stiffened trapezoidal profiled sheeting

The previous approach adopts the hypothesis that improved TPS beams are designed from a semi-automatic procedure based on critical moments criteria and many geometrical parameters. That methodology has two obvious limitations: (i) there is no guarantee that the solution found to be the global maximum of the proposed fitness function, and (ii) the detailed "best solution" strength study (where three modes have roughly the same critical moment value) does not reveal the influence of possible modal interactions. In other words, it is not clear for us whether the "best solution" is the same when the profile improvement process is based on strength criteria, considering L-D interaction.

The Local mode starts to manifest in the B-U interval of FEM nonlinear analysis, according to the examples presented on Fig. 9(c,d) and Fig. 9(e,f). The ultimate strengths of selected models (Franco et al 2016) have been evaluated by Ansys to investigate (as a first approach) L-D interaction. Results have been plotted over graphs of type M_{crj} xVar_i and M_{Rj}xVar_i, where M_{crj} is the jth buckling mode (obtained by CUFSM and confirmed by Ansys), M_{Rj} is the strength (Ansys evaluation) associated with the jth buckling mode and Var_i is the ith geometric variable of the profile.

From Fig. 10, 11 and 12 it is noted that M_{cr}^{BD} is not dominant, except under very specific conditions. However, M_R^{BD} seems to be the most important criteria for beam design of this family of geometries, in any case. The Fig. 10 compares critical moments and strength (obtained by FEM) with the number and distribution of stiffeners in the profile. Note that, from Fig. 10(a), McrBL≈M_{cr}^{BDW}, where the number of stiffeners in the web is equal to two (N_2 = 2). From Fig. 10(b), $Mcr^{BL}≈M_{cr}^{BD}$, where there is only one stiffener in the bottom flange (N_3 = 1). The Fig. 10(c) shows that, for the suitable Attractor value (At = 1) and other parameters, results $M_{cr}^{BL}≈M_{cr}^{BDW}≈M_{cr}^{BD}$. Strength erosion is not evidenced where R_{DL}≈1. On the other hand, where M_{cr}^{BL} is dominant, there is a tendency of reduction on values of M_R^{BDW} and M_R^{BD}.

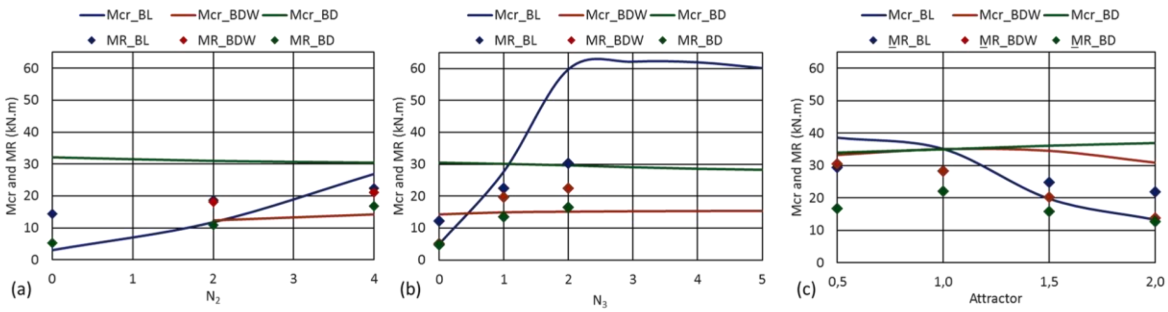

Figure 10: Sensibility analysis of stiffeners number and distribution: (a) web stiffeners, (b) bottom flange stiffeners, (c) web stiffeners distribution.

The Fig. 11 shows the comparison between M_{cr} and M_R once is given the variation of the geometric parameters in the stiffener. In Fig. *11(a)*, it is found that M_{cr}^{BL}≈M_{cr}^{BDW}, for w_{incl}=15mm and M_{cr}^{BDW}≈M_{cr}^{BD} for w_{incl}=20mm. Again, (i) strength erosion is not evidenced where R_{DL}≈1, and (ii) the variation rate of the M_R for distortional modes is reduced in the interval where the Local mode becomes dominant. This behavior is not clearly noticed in Fig. 11(b,c), which we attribute to the Local mode domination (or very close to it) in both intervals.

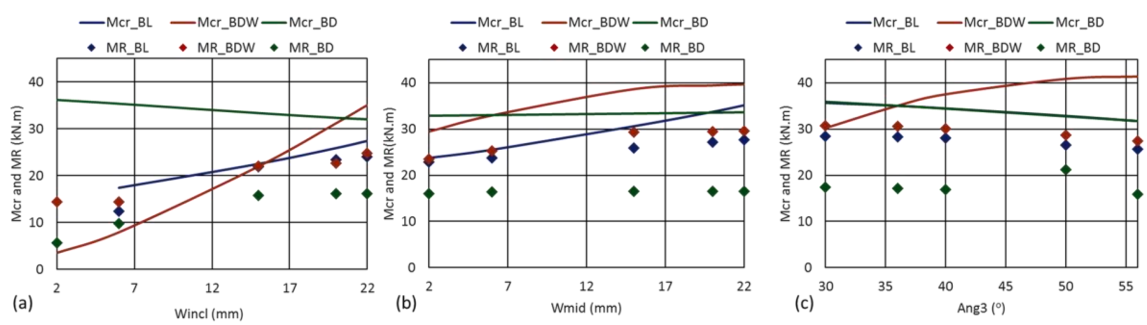

Figure 11: Sensibility analysis of stiffener parameters: (a) inclined wall width, (b) intermediate wall width, (c) angle between stiffeners walls.

The Fig. 12 shows three examples of the influence of TPS geometric parameters on M_{cr} and M_R. In Fig. 12(a), it is observed that M_{cr}^{BD} is maximum for ϴ≈70, while M_R^{BD} is maximum for ϴ≈80. As a hypothesis, we assign this difference between the maxima to the improved distance between the M_{cr}^{BL} and M_{cr}^{BD} curves.

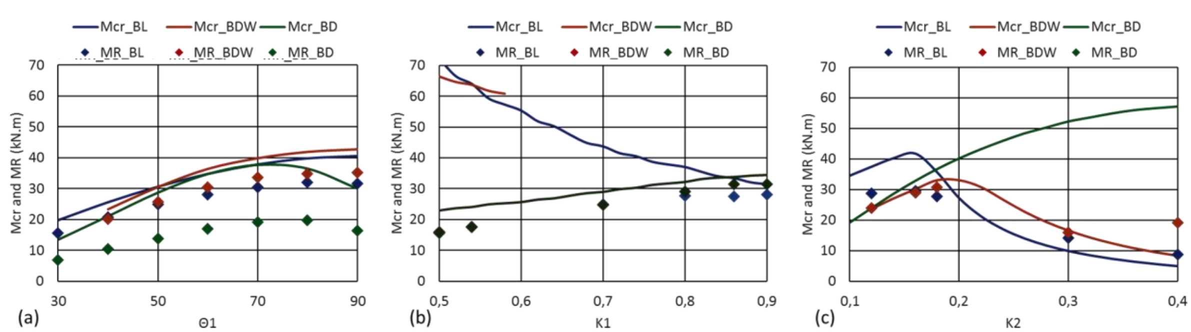

Figure 12: Sensibility analysis of TPS parameters: (a) angle between flange and web; (b) ratio between top web and coil length; (c) ratio between bottom flange and web

In Figs. 10 to 12 we assume hypotheses on the behavior of the strength associated with the distortional modes as a function of the preponderance of the Local mode, but we do not allow to generalize a design procedure for these profiles. Fig. 13, on the other hand, compares the ultimate strength obtained by FEM to the expression proposed by AISI Standard. In Fig. 13(a,b), the curves are close, but at Fig. 13(c) the standard curve is above the numerical results (against safety). In fact, AISI Standard offers a set of geometric constraints to TPS design, like the ratio h_0/t <203, where $\mathbf{h_0}$ is the height of the profile and **t** is the thickness of the walls. This restriction has been violated by semi-automatic process adopted in this study (see Fig. 7), allowing profiles more efficient than those pre-qualified by the MRD equations, according to AISI. (see Eq. 1)

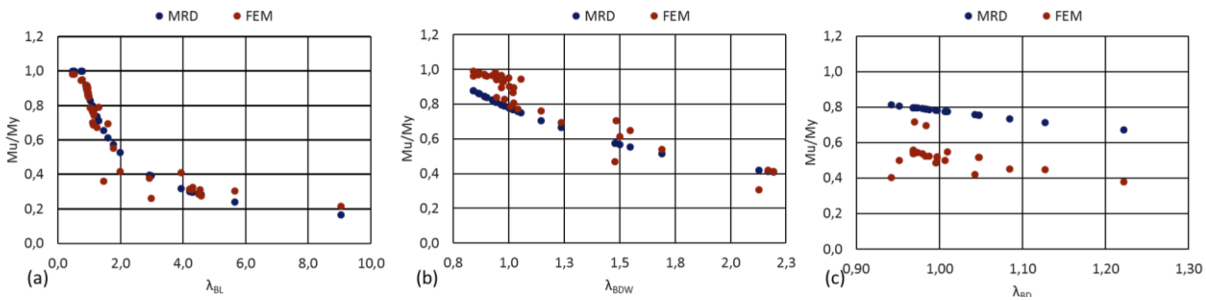

Figure 13: Comparison of results MRD (AISI) and FEM: (a) buckling mode BL; (b) buckling mode BDW; (c) buckling mode BD

$$M_R^{BL} = Wf_y \qquad \text{for} \quad \lambda_{BL} \leq 0.776 \qquad (1.1)$$
$$M_R^{BL} = (1\text{-}0.15/\lambda_{BL}^{0.8})\, Wf_y/\, \lambda_{BL}^{0.8} \qquad \text{for} \quad \lambda_{BL} > 0.776 \qquad (1.2)$$
$$M_R^{BD} = Wf_y \qquad \text{for} \quad \lambda_{BD} \leq 0.673 \qquad (1.3)$$
$$M_R^{BD} = (1\text{-}0.22/\lambda_{BD})\, Wf_y/\, \lambda_{BD} \qquad \text{for} \quad \lambda_{BD} > 0.673 \qquad (1.4)$$

The Fig. 14, on the other hand, shows the comparison of the same results obtained in FEM with the strength curve proposed by authors in Eq. 2.1 to 2.6. It should be noted that this curve is a preliminary result and that an experimental campaign to validate this equation has not yet been carried out.

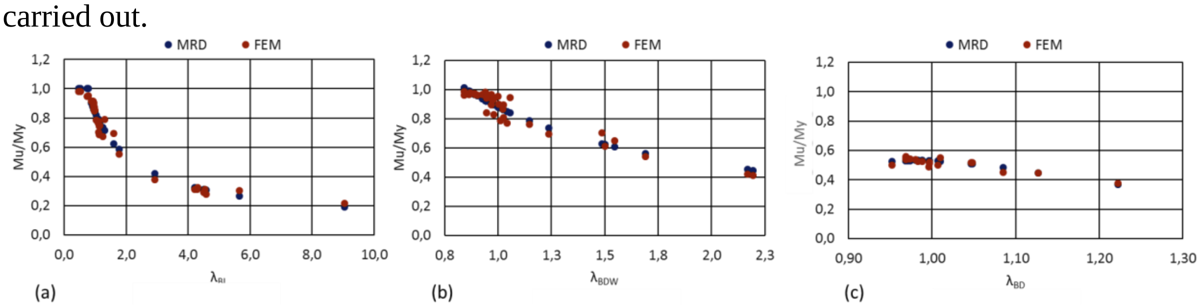

Figure 14: Comparison of results MRD (proposed) and FEM: mode (a) BL, (b) BDW, (c) BD

$$M_{R\_BL} = Wf_y \qquad \text{for} \quad \lambda_{BL} \leq 0.776 \qquad (2.1)$$
$$M_{R\_BL} = (1\text{-}0.16/\lambda_{BL}^{0.74})Wf_y/\, \lambda_{BL}^{0.74} \qquad \text{for} \quad \lambda_{BL} > 0.776 \qquad (2.2)$$
$$M_{R\_BDW} = Wf_y \qquad \text{for} \quad \lambda_{BDW} \leq 0.673 \qquad (2.3)$$
$$M_{R\_BDW} = (1\text{-}0.12/\lambda_{BDW}^{0.95})Wf_y/\, \lambda_{BDW}^{0.95} \qquad \text{for} \quad \lambda_{BDW} > 0.673 \qquad (2.4)$$
$$M_{R\_BD} = Wf_y \qquad \text{for} \quad \lambda_{BD} \leq 0.673 \qquad (2.5)$$
$$M_{R\_BD} = (1\text{-}0.47/\lambda_{BD}^{3.7})Wf_y/\, \lambda_{BD}^{3.7} \qquad \text{for} \quad \lambda_{BD} > 0.673 \qquad (2.6)$$

6. "Best geometry" from strength-based procedure

In recent work, Franco and Batista (2017) have proposed a semi-automatic procedure in order to improve TPS based on critical moments. This section briefly describes the obtained results from a modified version of this methodology. At this experiment, the fitness function is given by a strength curve (Eq. 2). Therefore, the implementation obeys L-D interaction for TPS proposed in last section.

The Fig. 15 presents M_R^{TC} and M_R^{BC} as functions of TPS geometric parameters. In Fig. 15 (a, b, c), it is noted that the number of stiffeners in the top flange, bottom flange and web do not affect significantly the strength. In a way, the width and the angle of stiffener walls have little influence on M_R^{BC} and M_R^{TC} (see Fig. 15 (d, e, f)). Previous parametric studies (Franco and Batista 2017) indicate that these variables affect more the BL and BDW modes than BD mode. However, Fig. 13 and Eq. 2 suggest that M_R^{BD} is dominant for $M_{cr}^{BL} \approx M_{cr}^{BDW} \approx M_{cr}^{BD}$ cases. Thus, according to the results obtained by Eq. 2, the improvement of the profile strength should prioritize parameter that affect M_{cr}^{BD}. In Fig. 15 (g, h), k_1 and k_3 are geometric parameters related to the ratio between the web widths and flanges. According to previous works (Franco and Batista 2017), these parameters are related to the variation of M_{cr}^{BD}. Fig. 15 (g) indicates that strength values are maximal (M_R^{BC} = 20.0 kNm and M_R^{TC} = 40.0 kNm) where $k_1 = 0.82$. It is an increase of respectively 25% (20 / 16 = 1.25) and 53% (40/26) over the previous results. Fig. 15 (h) presents increasing of 5% (21/20) in M_R^{BC}, for $k_3 = 0.16$. The Fig. 15(h) also demonstrates Eq. 2 is valid only within limits, not defined in this paper.

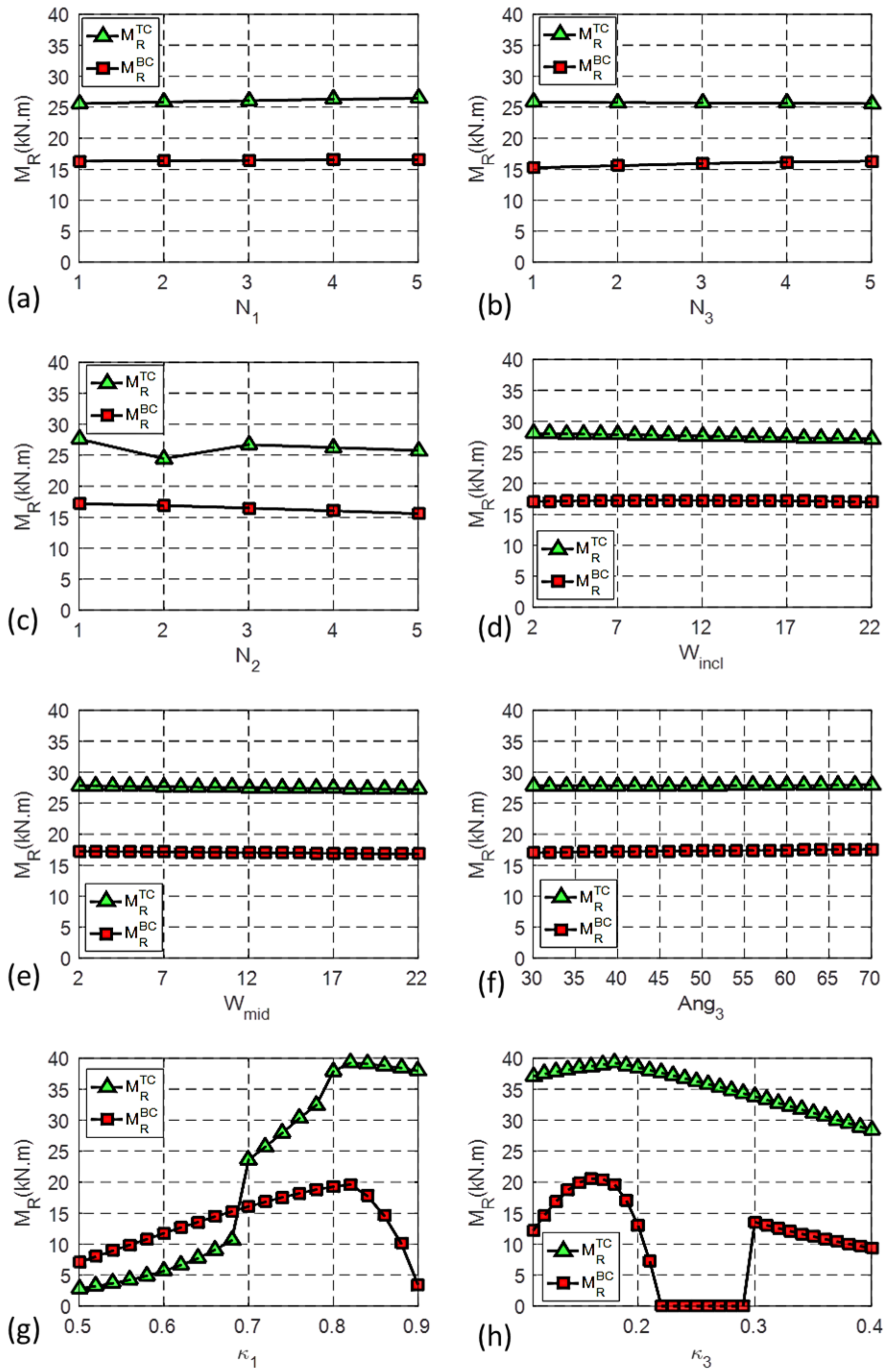

Figure. 15: Flexural strength (M_R^{BC} and M_R^{TC}) and geometric parameters of stiffened trapezoidal profiled sheeting sections: (a) number of stiffeners on top flange, (b) number of stiffeners on bottom flange, (c) number of stiffeners on web, (d) width of stiffeners inclined wall, (e) width of stiffeners middle wall, (f) angle between stiffeners walls, (g) ratio between top flange and coil width (h) ratio between bottom flange and web width.

7. Conclusions

Following previous investigation that developed rational method to obtain improved stiffened trapezoidal profiled sheeting sections, initially based on the elastic buckling performance, the present results are addressed to estimate the flexural strength, M_R^{BC}. The shell FEM numerical model included initial geometrical imperfections, ductile material properties and allowed identifying the ultimate bending moment associated with the inelastic collapse mechanism. The obtained results show correspondence between critical buckling modes and the nonlinear behavior until the ultimate loading condition. On the other hand, for some cases it was identified changing of the deformed shape of the trapezoidal member at the final stage of loading steps, as is the case shown in Fig. 9(e): distortional *BDW* changes to local *BL*. These results are affected by buckling modes interaction, as observed before in the buckling signature curve in Fig. 8. DSM equations for direct computation of the bending moment strength M_R^{BC} were applied for both local and distortional buckling. Comparison between DSM and FEM results indicated good agreement for five of the total number of six examined cases.

Different ratios among D and L modes have been evaluated by a non-linear FEM analysis to estimate L-D interaction and a very initial approach was carried out to define a strength curve for stiffened trapezoidal profiled sheeting sections. This curve is the core of a proposed method based on strength performance and suggests M_{cr}^{BD} is dominant in improvement process. The "best" shape given by elastic buckling performance method presents higher flexural bending values (Tab. 02) than strength curve method (Eq.2 and Fig 15(h)). For sure, additional numerical and experimental results are needed to permit more general conclusions.

Acknowledgments

The authors are grateful to CNPq, National Council for the Scientific and Technological Development, for the support of the Master scholarship of the second author.

References

Martins, A.D., Dinis, P.B., Camotim, D. (2017) "Local-distortional interaction in cold-formed steel beams: Behaviour, strength and DSM design", *Thin-Walled Structures* 119 879-901.

Franco, J.M.S., Batista, E. M. (2017) "Buckling behavior and strength of thin-walled stiffened trapezoidal CFS under flexural bending". *Thin-Walled Structures* 117 268-281.

AISI. (2006) "Direct Strength Method (DSM) Design Guide". *American Iron and Steel Institute*.

Eurocode 3. (2004) "Design of steel structures. Part 1-3: General rules, Supplementary rules for cold-formed members and sheeting". Brussels.

Chomsky, N. (1972) "Syntatic Structures", *Mouton and CO*, Netherlands.

Stiny, G., Gips, J. (1972) "Shape Grammars and Generative Specification of Painting and Sculpture", *Auerbach Publications*, USA

Franco J.M.S., Duarte, J.P., Batista, E.M., Landesmann, A. (2014) "Shape grammar of steel cold-formed sections based on manufacturing rules", *Thin-Walled Structures* 79 218-232.

Li, Z., Schafer, B. W. (2010) "Buckling analysis of cold-formed steel members with general boundary conditions using cufsm: conventional and constrained finite strip methods*", Proceedings of the 20th Int. Spec. Conf. on Cold-Formed Steel Structures*.

SAS (Swanson Analysis Systems Inc.) (2015). "ANSYS Mechanical APDL Theory Reference" (version 16.0)

Ádány, S. (2004). "Buckling mode classification of members with open thin-walled crossections by using the finite strip method". Research Report, John Hopkins University.